analytical chemistry

Article

Cite This: Anal. Chem. 2019, 91, 13290−13296

pubs.acs.org/ac

Photothermal Microfluidic Sensing Platform Using Near-Infrared Laser-Driven Multiplexed Dual-Mode Visual Quantitative Readout

Guanglei Fu,*[,†] Yabin Zhu,[†] Kui Xu,[†] Weihua Wang,[‡] Ruixia Hou,[†] and Xiujun Li*[,§]

[†]Biomedical Engineering Research Center, Medical School of Ningbo University, Ningbo, Zhejiang 315211, P. R. China

[‡]The Affiliated Hospital of Medical School of Ningbo University, Ningbo, Zhejiang 315020, P. R. China

[§]Department of Chemistry and Biochemistry, University of Texas at El Paso, 500 West University Avenue, El Paso, Texas 79968, United States

Supporting Information

ABSTRACT: The application of different sensing principles in microfluidic devices opens up further possibilities for the development of point-of-care testing (POCT). Herein, the photothermal sensing principle is introduced in microfluidic paper-based analytical devices (μPADs) to develop a photothermal microfluidic sensing platform using near-infrared (NIR) laser-driven multiplexed dual-mode visual quantitative readout. Prussian blue (PB) as the analyte-associated photothermal agent was in situ synthesized in thermoresponsive poly(*N*-isopropylacrylamide) hydrogels to serve as the on-chip photothermal sensing element. The NIR laser-driven photothermal effect of PB triggered not only on-chip dose-dependent heat generation but also phase transition-induced dye release from the hydrogels, simultaneously enabling both thermal image- and distance-based dual-mode visual quantitative readout of the analyte concentration in a multiplexed manner. Both the on-chip temperature elevation value of the hydrogels and the traveling distance of released dye solutions were proportional to the concentration of PB. With the detection of silver ions in environmental water as a proof-of-concept study, the photothermal μPAD can detect silver ions at a concentration as low as 0.25 μM with high selectivity and satisfactory accuracy. The photothermal microfluidic sensing platform holds great potential for POCT with promising integratability and broad applicability, owing to the combination of synergistic advantages of the photothermal sensing principle, μPADs, and photothermally responsive hydrogels.

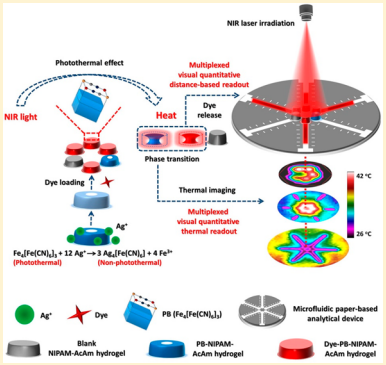

Photothermal effect has been a hot research subject in various fields, such as energy storage and photics.[1,2] When exposed to external lights of certain wavelengths, photothermal materials can perform the light-to-heat energy transformation through different mechanisms,[3,4] which is particularly promising for photothermal ablation of cancer cells.[3,4] Very recently, the application of the photothermal effect is extended to the field of bioassay,[5,6] exhibiting tremendous potential for point-of-care testing (POCT). For instance, our research group had exploited the photothermal effect in immunoassays to enable the transduction of conventional assay signals into heat signals that can be simply monitored by using a digital thermometer in a quantitative way.[5,6] However, the potential applicability of the photothermal sensing strategy in POCT has to be compromised in terms of integratability, operability, and deliverability of the assay approach. Taking advantages of laser pointers for lab-on-a-chip operations (e.g., ease of miniaturization and spatiotemporal controllability), the application of the photothermal sensing principle in lab-on-a-chip devices, especially in microfluidic devices, might offer new opportunities to develop a novel sensing platform with improved applicability in POCT.

Microfluidic paper-based analytical devices (μPADs) have become increasingly powerful analytical tools because of the advantages of inexpensiveness, portability, and operational simplicity.[7−9] Various sensing principles, such as fluorescence and electrochemistry, have been adopted in μPADs for quantitative analysis.[10,11] Despite great research efforts, several challenges, especially the relying of readout methods on bulky analytical instruments, are usually encountered by these μPADs in quantitative POCT.[12] Although the visual distance-based quantitative readout method has been adopted in μPADs, the requirement of complex off-chip sample-pretreatment and on-chip liquid-handling procedures remains a severe challenge. In combination with intelligent sensing elements, the application of the photothermal sensing principle in μPADs holds the possibility to compensate for these limitations in a synergistic fashion.

Stimuli-responsive hydrogels have shown enormous potential as intelligent sensing elements in microfluidic devices.[10] In response to external stimulus, responsive hydrogels undergo "smart" three-dimensional (3D) structural changes that can be displayed in different sensing signals.[13,14] Yang et al. had integrated intelligent aptamer-cross-linked hydrogels in multi-

Received: September 5, 2019
Accepted: September 11, 2019
Published: September 11, 2019

DOI: 10.1021/acs.analchem.9b04059
Anal. Chem. 2019, 91, 13290−13296

Scheme 1. Photothermal Microfluidic Sensing Principle of the μPAD[a]

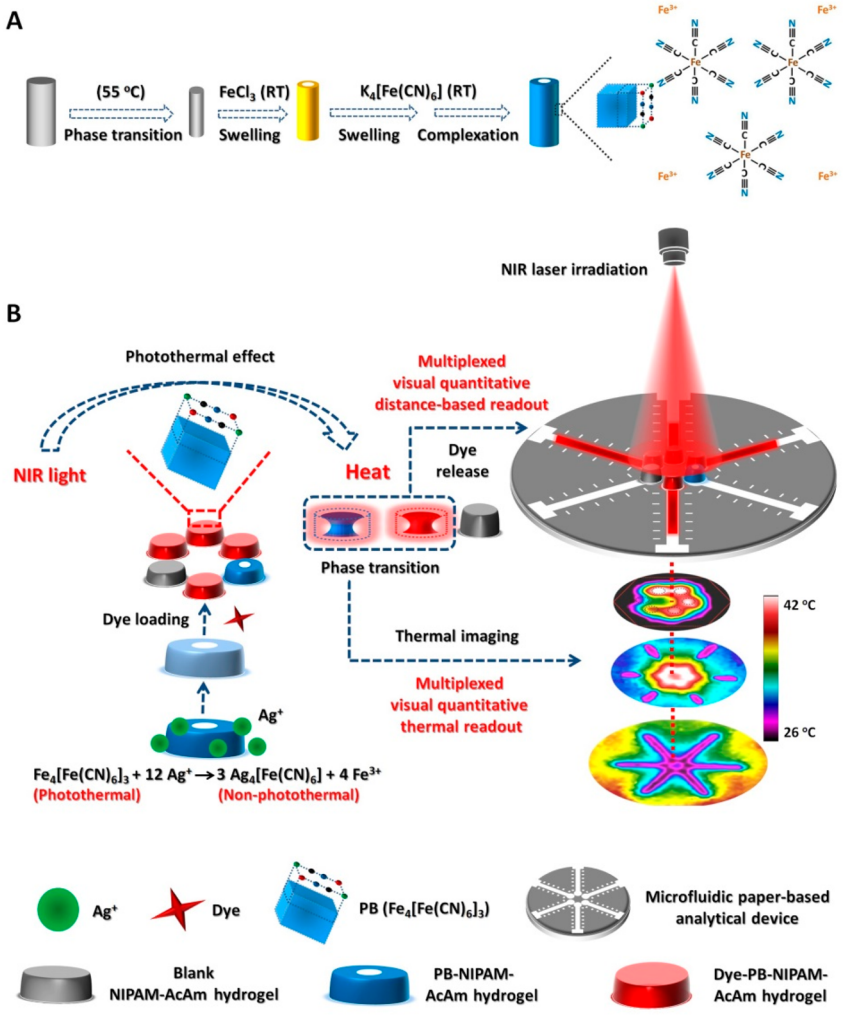

[a]Schematic illustration of (A) preparation route of the photothermally responsive hydrogel and (B) microfluidic sensing principle using the dual-mode visual quantitative readout method.

ple μPADs to initiate specific molecular recognitions.[10,12] As a new type of responsive hydrogels synthesized from the composition of photothermal agents with thermoresponsive hydrogels, the photothermally responsive hydrogels have been employed as photoresponsive microvalves to control fluid flow in microfluidic devices.[15] Upon near-infrared (NIR) laser irradiation, sensitive structural collapse of the hydrogels could be triggered, resulting in the release of liquids that can be quantitatively associated with the concentration of the photothermal agents. These features make the photothermally responsive hydrogels particularly promising as intelligent sensing elements in microfluidic devices.

Herein, the photothermal sensing principle is introduced in μPADs for the development of a new microfluidic sensing platform using NIR laser-driven multiplexed dual-mode visual quantitative readout. Photothermally responsive hydrogels synthesized from the composition of Prussian blue (PB) and thermoresponsive poly(*N*-isopropylacrylamide) (NIPAM) hydrogels are integrated on the μPAD to serve as the photothermal sensing elements (Scheme 1). In response to NIR laser irradiation, analyte-associated photothermal effect of PB triggers not only dose-dependent heat generation but also phase transition-induced dye release from the hydrogel on the μPAD, simultaneously enabling thermal image- and distance-based dual-mode visual quantitative readout of the analyte concentration in a multiplexed manner. As a proof-of-concept study, the photothermal μPAD was utilized to quantify silver ions in environmental water. As far as we know, this work serves as the first attempt to exploit the photothermal sensing principle in μPADs to develop the photothermal microfluidic sensing platform. Given that affordable miniaturized pen-style laser arrays and tiny cellphone-integrable thermal imaging accessories including cellphone thermal analytical apps are widely commercialized, the integratability of the microfluidic sensing platform is of great promise. More importantly, a great number of conventional off-chip colorimetric and spectroscopic assay systems can be flexibly introduced into this sensing platform with broad applicability. Hence, the new microfluidic sensing platform holds tremendous potential for POCT, owing to the combination of the aforementioned synergistic advantages of the photothermal sensing principle, μPADs, and photothermally responsive hydrogels.

EXPERIMENTAL SECTION

Materials and Instruments. NIPAM was acquired from Sigma-Aldrich. An 808 nm laser system (New Industries

DOI: 10.1021/acs.analchem.9b04059
Anal. Chem. 2019, 91, 13290−13296

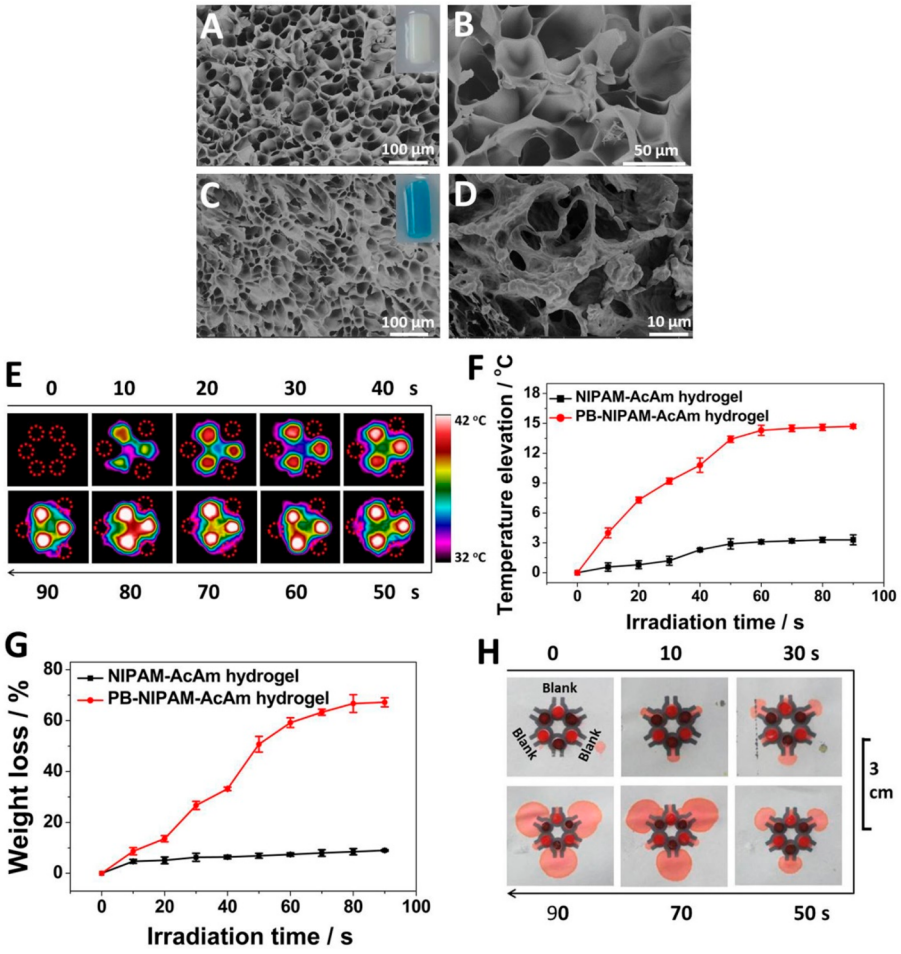

Figure 1. Off-chip morphological and photothermal characterization. Scanning electron microscopic images of blank (A, B) and composite (C, D) hydrogels; (E) thermal images after laser irradiation of hydrogels for varying times; (F) temperature changes of hydrogels; (G) weight changes of hydrogels; (H) pictures of hydrogels on the paper substrates after the irradiation. (inset) Pictures of corresponding hydrogels. Dotted circles indicate locations of the blank hydrogels. Error bars in all figures represent standard deviations (n = 3).

Optoelectronics Technology Co., Ltd.) was employed to conduct the irradiation experiments (see details in Supporting Information).

NIR Laser-Driven On-Chip Dual-Mode Visual Quantitative Readout. The rod-shaped hydrogels were cut into multiple slices (see preparation and size details in Supporting Information), followed by drying of the hydrogel slices on filter papers. To trigger the on-chip dual-mode visual quantitative readout, the hydrogel slices loaded on the central irradiation zone of the μPAD (see fabrication and Ag^+ detection procedures in Supporting Information) were irradiated by the laser at different powers. The size of the laser spot was adjusted to 2.6 cm to enable the uniform coverage of the irradiation zone. After the laser irradiation, on-chip temperature changes and the dye-traveling distance were recorded for the thermal image- and distance-based visual quantitative readout, respectively (see readout details in Supporting Information). Unless otherwise indicated, laser irradiation was performed with a power density of 0.38 W·cm^{-2}.

RESULTS AND DISCUSSION

Off-Chip Photothermal Characterization. To prepare the photothermally responsive hydrogels, PB was synthesized in thermoresponsive poly(*N*-isopropylacrylamide)−acrylamide (NIPAM-AcAm) hydrogels through an in situ synthesis route. By controlling the phase-transition behavior of the blank hydrogels at temperatures above and below their lower critical solution temperature (LCST), $FeCl_3$ and potassium ferrocyanide aqueous solutions were successively incorporated into the hydrogels to enable the in situ complexation of PB in the hydrogel networks. The as-obtained composite hydrogel (i.e., PB-NIPAM-AcAm) exhibited the typical color of PB (Figure 1C). The production of PB in the composite hydrogel was further confirmed by Fourier transform infrared spectroscopy (Figure S1).

As shown in Figure 1A−D, uniform 3D macroporous networks were observed in scanning electron microscopic (SEM) images of both the blank and the composite hydrogels. These polymerized networks can incorporate large amounts of liquids at the swollen state.[13,14,16] In comparison with the blank hydrogel, the composite hydrogel exhibited networks of smaller pore size (i.e., 20 to ∼38 μm in diameter) with rougher polymer walls (Figure 1C,D). The deposition of numerous particles of ∼1.5−3.0 μm in diameter can be clearly observed on the polymer walls in the composite hydrogel. These particles were concluded to be PB microcrystals as a result of the in situ complexation reaction between $FeCl_3$ and potassium ferrocyanide in the polymer pores.

PB in the composite hydrogel was expected to serve as the analyte-associated photothermal agent[5,17] to trigger the phase

DOI: 10.1021/acs.analchem.9b04059
Anal. Chem. 2019, 91, 13290−13296

transition of the hydrogels. Meanwhile, dye solutions as the nonphotothermal quantitative indicator were loaded into the hydrogels. The optical absorption properties of food dye and PB in the NIR region were characterized by UV−vis absorption spectroscopy (Figure S2). PB NPs showed significant optical absorption in the NIR region,[17] whereas the dye showed no apparent optical absorption in this region. The result demonstrated that only PB acted as the photothermal component in the composite hydrogel without any photothermal interference from the dye.

To investigate the NIR laser-driven phase-transition behavior of the hydrogels, an 808 nm laser was utilized to irradiate the hydrogels for various times. Multiple blank and composite hydrogel pieces were loaded alternately in a circular shape on a patterned chromatography paper substrate (Figure 1H). The diameter of the laser spot was adjusted to cover all hydrogels uniformly. Interestingly, thermal imaging of the hydrogels was successfully implemented in a multiplexed manner with the vivid display of thermal information on multiple hydrogels in a single image (Figure 1E,F). In each thermal image, identical thermal display was observed from the same type of the hydrogels, suggesting the homogeneous synthesis of PB in the composite hydrogels as well as the uniform distribution of the laser beam. With the increasing irradiation time from 0 to 90 s, the composite hydrogels showed dramatically increased temperature with a significant increase value of 14.3 °C at 60 s. The blank hydrogels exhibited minor temperature elevations of lower than 3.3 °C, which were unobservable in the thermal images at the current thermal scale.

Phase transition of the NIPAM hydrogels occurs at temperatures higher than their LCST.[13,16,18] To confirm the photothermal effect-induced phase-transition behavior, weight loss of the hydrogels was monitored at varying irradiation times (Figure 1G). With the increasing irradiation time, the composite hydrogels displayed progressively increased weight loss up to 68% of their initial value at 90 s, whereas the blank hydrogels showed minor weight losses of lower than 9.0%. The NIPAM hydrogels had been demonstrated to have an LCST of ∼34.4 °C that can be slightly altered upon the doping of comonomers or nanomaterials.[14] Hence, it was concluded that the composite hydrogels started to reach the LCST at the irradiation time of 20 s (Figure 1F) when drastic phase transition and weight loss occurred. The weight-loss behavior was further confirmed by volume changes of the hydrogels and the progressive dye-release phenomenon on the paper substrate (Figure 1H). The sensitive photothermal effect-triggered phase-transition behavior of the composite hydrogel made it particularly promising as the photothermal sensing element on μPADs.

Principle of On-Chip Dual-Mode Visual Quantitative Readout. To study the applicability of the composite hydrogel as the photothermal sensing element on μPADs, a disklike μPAD was designed as shown in Figure 2. The μPAD consisted of a central irradiation zone and multiple straight channels, which were designed for thermal image- and distance-based visual quantitative readout, respectively. The hydrogels were treated by different stimuluses on the μPAD. Because of the distinct temperature elevation (i.e., 10 °C) of the hydrogels during the incubation in water bath (40 °C), obvious dye release and migration of dye solutions in the channels were observed from both the blank and the composite hydrogels. After the laser irradiation for only 60 s,

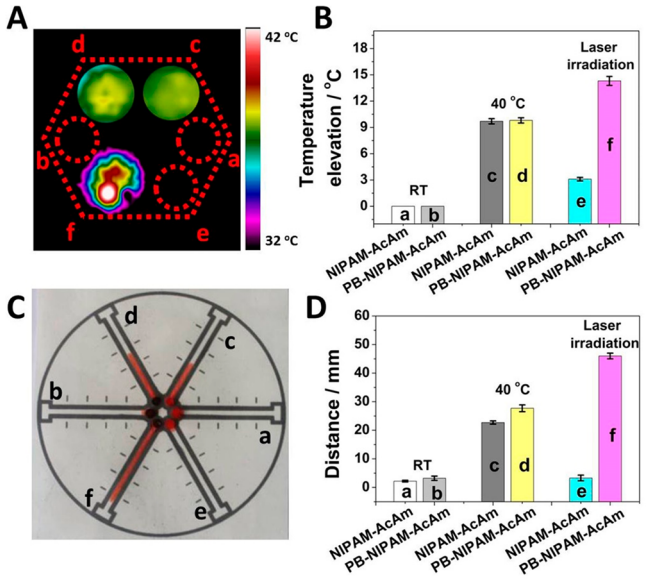

Figure 2. Implementation of NIR laser-driven on-chip dual-mode visual quantitative readout. (A) Merged thermal images of the hydrogel-loaded μPAD after various treatments. (B) Thermal variations of the hydrogels. (C) Picture of the hydrogel-loaded μPAD after various treatments. (D) Traveling length of dye solutions. RT: storage at room temperature for 10 min; 40 °C: storage for 6.0 min at 40 °C. Laser irradiation: exposure to the laser for 60 s.

the composite hydrogel displayed a dramatic on-chip temperature increase of 14.3 °C and a dye-traveling length of 46 mm, whereas the blank hydrogel showed a negligible dye-traveling length of 3.3 mm. The thermal readout results corresponded well with that of the distance-based readout method, indicating the direct correlation between these two readout methods.

In our previous works,[5,6] the photothermally induced temperature increase values were proved to be linearly associated with the concentrations of photothermal agents in certain ranges. In addition, it was demonstrated that the movement length of the dye solution on the μPAD was proportional to the solution volume in a certain range (Figure S3). Hence, by using the composite hydrogel as the analyte-associated photothermal sensing element on the μPAD, it was possible to quantitatively display the sensing signal with the dual-mode visual readout method.

On-Chip Photothermal Sensing Performance. The thermal image-based readout method was utilized to monitor the photothermal sensing process on the μPAD. Six uniform pieces of the composite hydrogels that were prepared in parallel were irradiated on the μPAD. As shown in Figure 3A, the composite hydrogels exhibited uniform temperature elevations of ∼13.8 °C after the irradiation, resulting in clear hexagonal-shaped thermal display of the hydrogels in the thermal image. At the meantime, release of dye solutions with a lower temperature (i.e., 29.3 °C) from the hydrogels can be clearly observed. After the laser irradiation, the temperature of the hydrogels decreased rapidly to 27.2 °C within 30 s and gradually returned to their initial temperature. Dye solutions in the channels formed a clear starfishlike shape in the thermal images. These results demonstrated the capability of the thermal readout method for quantitative thermal analysis of the photothermal sensing performance.

To investigate the influence of irradiation time on the sensing performance, the hydrogel pieces were irradiated on

DOI: 10.1021/acs.analchem.9b04059
Anal. Chem. 2019, 91, 13290−13296

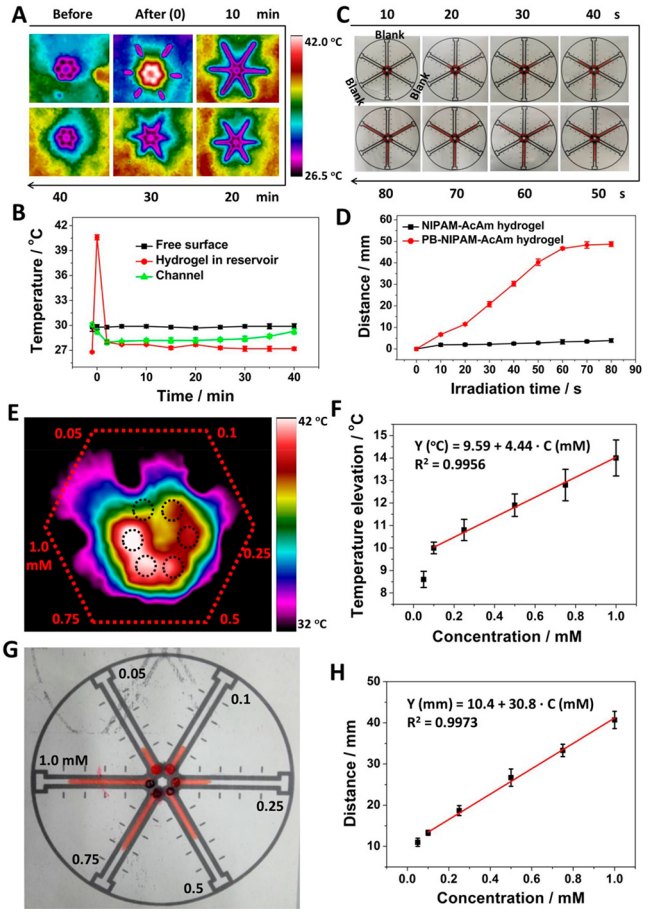

Figure 3. Multiplexed dual-mode visual quantitative readout of the sensing performance. (A) Thermal images of the μPAD recorded at intervals after the irradiation (50 s). (B) Thermal variations of the composite hydrogel, channels, and device surface at different times. (C) Pictures of the hydrogel-loaded μPAD after the irradiation for varying times. (D) Dye-traveling length at different irradiation times. (E) Thermal image of the hydrogels synthesized from varying $FeCl_3$ concentrations after the laser irradiation (50 s). (F) Relationship between temperature increase value and $FeCl_3$ concentration. (G) Picture of the hydrogel-loaded μPAD after the irradiation. (H) Relationship between dye-traveling length and $FeCl_3$ concentration.

the μPAD for different times and analyzed using the distance-based readout method. The composite hydrogels exhibited progressively elevated dye-traveling distance (i.e., 47 mm at 60 s) with increasing irradiation time, while the blank hydrogels showed minor dye-traveling length at various times (Figure 3C,D). The above distance-based readout results corresponded well with that of Figure 1G (i.e., weight loss), suggesting the consistence of the distance-based readout results with the phase-transition behavior of the hydrogels. The photothermal sensing performance displayed a laser power-dependent character (Figure S4).

The influence of PB concentration on the sensing performance was studied using composite hydrogels prepared from varying concentrations of $FeCl_3$ in the synthesis of PB. With the clear thermal display of multiple hydrogels in a single thermal image after the irradiation (Figure 3E), increasing temperature elevations were monitored with the increase of $FeCl_3$ concentration, attributed to the synthesis of increasing concentrations of PB in the composite hydrogels. The temperature increase value as well as the on-chip dye-traveling length was linearly dependent on the $FeCl_3$ concentration in the range from 0.1 to 1.0 mM (Figure 3E–H). These results indicated the successful quantitative readout of the photothermal sensing performance of the composite hydrogel using the dual-mode readout method. By quantitatively associating the production or decomposition of PB in the composite hydrogel with target analytes, the analytes can be quantified on the photothermal μPAD in a multiplexed manner. The composite hydrogel showed good reproducibility and remarkable recovery for photothermal sensing on the μPAD (Figures S5 and S6).

On-Chip Multiplexed Determination of Silver Ions. To verify the feasibility of the photothermal μPAD for practical analytical application, the determination of silver ions in environmental water was chosen as a proof-of-concept study. On the basis of a dissolution–precipitation equilibrium mechanism employing the Ag^+-induced material conversion from PB ($Fe_4[Fe(CN)_6]_3$) to colorless silver ferrocyanide ($Ag_4[Fe(CN)_6]_3$), PB had been reported as a sensing probe for spectrophotometric determination of Ag^+.[19] Herein, by using the composite hydrogel as the on-chip photothermal sensing element, the assay was introduced in the photothermal μPAD to enable spectrophotometer-free multiplexed visual quantitative detection of Ag^+. The Ag^+-induced material conversion from photothermal PB to nonphotothermal silver ferrocyanide was confirmed by UV–vis adsorption spectroscopy (Figure S7).

The sample pretreatment was simply performed through incubation of the composite hydrogels in Ag^+ solutions. The composite hydrogels exhibited increasingly faded color after the incubation with increasing concentrations of Ag^+ solutions (Figure 4), indicating the decrease of PB concentration in the

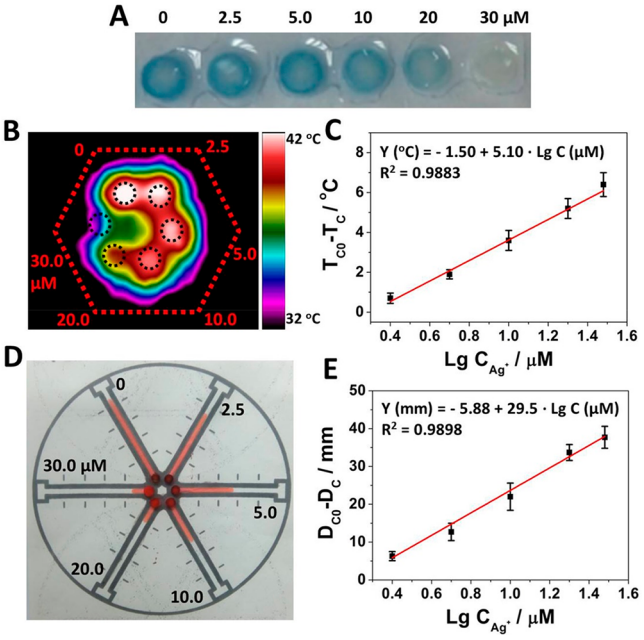

Figure 4. Determination of Ag^+ on the photothermal μPAD. (A) Picture of the composite hydrogels after incubation in various concentrations of Ag^+ solutions. (B) Thermal image of the hydrogel-loaded μPAD after the irradiation for 60 s. (C) Relationship between temperature increase value and logarithm of Ag^+ concentration. (D) Picture of the hydrogel-loaded μPAD. (E) Relationship between dye-traveling length and logarithm of Ag^+ concentration.

DOI: 10.1021/acs.analchem.9b04059
Anal. Chem. 2019, 91, 13290–13296

hydrogels as a result of the material conversion.[19] As expected, a progressive decrease in temperature of the hydrogels was monitored with increasing concentration of Ag^+ after the laser irradiation. Both the relative temperature variation value ($T_{C0} - T_C$) and the relative dye-traveling distance ($D_{C0} - D_C$) were proportional to the logarithm of Ag^+ concentrations in the range from 2.5 to 30 μM with limit of detection (LOD) (signal-to-noise ratio (S/N) = 3) of 2.2 and 2.0 μM, respectively. Although the LOD values were higher than that of the spectrophotometric method (i.e., 5.0 nM),[19] they were comparable to that of the previously reported colorimetric paper strip (i.e., 1.7 μM) employing off-chip accessories including a peristaltic pump, a flow cell, a scanner, waste collectors, and a computer.[20] Nevertheless, note that the detection limit can be further decreased by prolonging the pretreatment time of the composite hydrogel. For instance, Ag^+ can be quantified at a lower concentration of 0.25 μM upon the prolonging of incubation time of the composite hydrogel to 10 h (Figure S8). The dual-mode readout results were herein calibrated into relative variation values (i.e., $D_{C0} - D_C$ and $T_{C0} - T_C$), through which the influence of temperature on the readout results can be neutralized.

As the World Health Organization and U.S. Environment Protection Agency define the maximum acceptable concentration of Ag^+ in drinking water as 0.1 mg/L (i.e., 0.93 μM)[21] and 0.05 mg/L (i.e., 0.46 μM),[21,22] respectively, the developed photothermal μPAD can completely meet the requirement of detection threshold for practical environmental monitoring of Ag^+. In comparison with the colorimetric paper strip,[20] the photothermal μPAD is more advantageous for potential application in POCT, owing to its higher integratability, more direct distance- and thermal image-based visual quantitative readout without complex data-processing approaches (e.g., computer-based analysis of color intensity), and simpler sample pretreatment without the aid of any liquid-handling accessories (e.g., peristaltic pumps, pipettes, and flow cells).

To evaluate the selectivity of the μPAD for determination of Ag^+, other interfering metal ions were tested as the negative control as shown in Figure 5. No noticeable color changes were observed from these control hydrogels after the sample pretreatment, while the Ag^+-treated hydrogel exhibited an obviously degraded color due to the material conversion. In contrast to the same concentration of Ag^+ solution, the interfering metal ions led to both no significant relative temperature changes ($T_{C0} - T_C$) and negligible relative variations in the dye-traveling distance ($D_{C0} - D_C$) (Figure S9). These results demonstrated high selectivity of the photothermal μPAD for determination of Ag^+, due to the high specificity of the material conversion reaction.[19]

Validation of Practical Application of the Photothermal μPAD. To validate the photothermal μPAD for practical Ag^+ detection, real water samples collected from a local lake were tested on the μPAD. The water samples were spiked with different concentrations (i.e., 5.0, 10, and 20 μM) of standard Ag^+ solutions. After incubation with the composite hydrogels, Ag^+ concentrations in the water samples were quantified using the dual-mode readout method (Figure S10). It was found that the thermal image- and distance-based readout results were consistent with that of Figure 4. The analytical recoveries of the μPAD ranged from 95% to 102% (Tables S1 and S2), suggesting satisfactory accuracy of the photothermal μPAD.

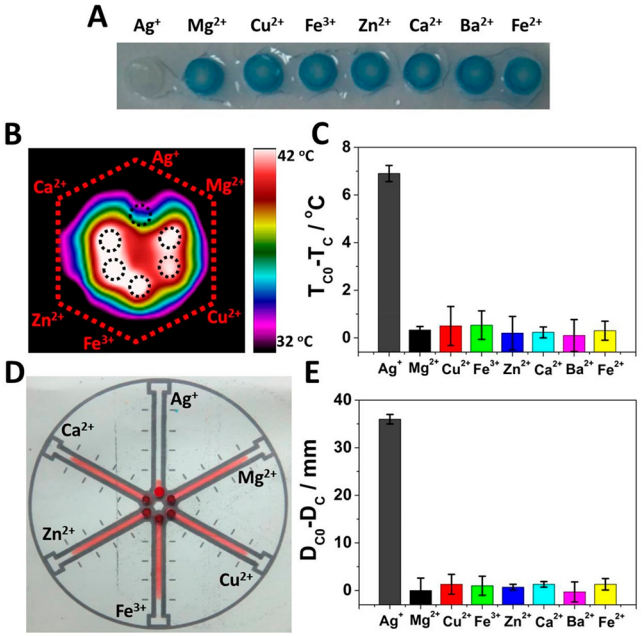

Figure 5. Selectivity of the photothermal μPAD. (A) Picture of the composite hydrogels after incubation in the same concentration (i.e., 30 μM) of different metal ion solutions. (B) Thermal image of the hydrogel-loaded μPAD after the laser irradiation for 60 s. (C) On-chip relative temperature changes ($T_{C0} - T_C$) of the hydrogels. (D) Picture of the hydrogel-loaded μPAD. (E) Relative changes in dye-traveling distance ($D_{C0} - D_C$).

Although the multiplexed testing of only six samples is demonstrated on the current photothermal μPAD, the testing capacity can be further improved even in a high-throughput format by flexibly modifying the microfluidic pattern, size of the laser spot, and structure of the microfluidic device. For example, besides the simple appropriate magnification of the size of the laser spot, the 3D foldable integration of multiple paper layers patterned with separate fluidic pathways offers an efficient way to meet the requirement of the increase in the sample quantity. On the basis of the on-demand variation of the photothermal sensing approach on the μPAD, the photothermal microfluidic sensing platform can work in flexible ways to implement different analytical tasks. In particular, the site of the specific sensing reaction can be transferred to the paper substrate instead of the thermoresponsive hydrogel. With the on-chip analyst-associated conversion between photothermal and non-photothermal materials on the paper substrate, blank thermoresponsive hydrogels can herein directly serve as the on-chip photothermal sensing elements.

CONCLUSIONS

The photothermal sensing principle is introduced in μPADs to develop a photothermal microfluidic sensing platform using NIR laser-driven multiplexed dual-mode visual quantitative readout. PB-actuated photothermally responsive hydrogels serve as the on-chip photothermal sensing elements. As a proof-of-concept study, the photothermal μPAD shows high selectivity and satisfactory accuracy for Ag^+ determination in real environmental water samples with a low LOD. In comparison with traditional μPADs, the new sensing platform enables instrument-free multiplexed dual-mode visual quantitative readout with simpler sample-pretreatment procedures.

DOI: 10.1021/acs.analchem.9b04059
Anal. Chem. 2019, 91, 13290−13296

Given that affordable miniaturized pen-style laser arrays and tiny cellphone-integrable thermal imaging accessories including cellphone thermal analytical apps are widely commercialized, the integratability of the photothermal microfluidic sensing platform is of great promise. We envision that the photothermal microfluidic sensing platform can be applied in a broad range of fields, such as environmental monitoring, food safety inspection, and medical diagnosis. For example, a great number of conventional off-chip spectroscopic and colorimetric assays employing 3,3′,5,5′-tetramethylbenzidine (TMB),[23] gold nanorods,[24,25] and PB[26,27] as the sensing probes that have also been developed as photothermal agents[5,6,17,28] can be flexibly introduced into this sensing platform to enable the multiplexed visual quantitative detection of various analytes. Hence, the photothermal microfluidic sensing platform shows great potential for POCT.

■ ASSOCIATED CONTENT

Supporting Information

The Supporting Information is available free of charge on the ACS Publications website at DOI: 10.1021/acs.analchem.9b04059.

Details of materials and instruments, hydrogel synthesis, fabrication of μPADs, Fourier transform infrared characterization, effect of laser power, reproducibility and recovery of the photothermal μPADs, and determination results of Ag^+ in real water samples (PDF)

■ AUTHOR INFORMATION

Corresponding Authors

*E-mail: fuguanglei@nbu.edu.cn. (G.-L.F.)
*E-mail: xli4@utep.edu. (X.-J.L.)

ORCID

Guanglei Fu: 0000-0002-8128-1224
Xiujun Li: 0000-0002-7954-0717

Notes

The authors declare no competing financial interest.

■ ACKNOWLEDGMENTS

We are grateful to the financial support from the National Natural Science Foundation of P. R. China (No. 81701790) and the U.S. NSF-PREM program (No. DMR 1827745).

■ REFERENCES

(1) Jung, H. S.; Verwilst, P.; Sharma, A.; Shin, J.; Sessler, J. L.; Kim, J. S. *Chem. Soc. Rev.* **2018**, *47*, 2280−2297.
(2) Xiao, J.; Jiang, H. *Acc. Chem. Res.* **2019**, *52*, 356−366.
(3) Song, X.; Chen, Q.; Liu, Z. *Nano Res.* **2015**, *8*, 340−354.
(4) Jaque, D.; Maestro, L. M.; Rosal, B. D.; Harogonzalez, P.; Benayas, A.; Plaza, J. L.; Rodriguez, E. M.; Sole, J. G. *Nanoscale* **2014**, *6*, 9494−9530.
(5) Fu, G.; Sanjay, S. T.; Dou, M.; Li, X. *Nanoscale* **2016**, *8*, 5422−5427.
(6) Fu, G.; Sanjay, S. T.; Zhou, W.; Brekken, R. A.; Kirken, R. A.; Li, X. *Anal. Chem.* **2018**, *90*, 5930−5937.
(7) Sanjay, S. T.; Fu, G.; Dou, M.; Xu, F.; Liu, R.; Qi, H.; Li, X. *Analyst* **2015**, *140*, 7062−7081.
(8) Martinez, A. W.; Phillips, S. T.; Whitesides, G. M.; Carrilho, E. *Anal. Chem.* **2010**, *82*, 3−10.
(9) Sun, J.; Xianyu, Y.; Jiang, X. *Chem. Soc. Rev.* **2014**, *43*, 6239−6253.
(10) Tian, T.; Wei, X.; Jia, S.; Zhang, R.; Li, J.; Zhu, Z.; Zhang, H.; Ma, Y.; Lin, Z.; Yang, C. J. *Biosens. Bioelectron.* **2016**, *77*, 537−542.
(11) Cate, D. M.; Adkins, J. A.; Mettakoonpitak, J.; Henry, C. S. *Anal. Chem.* **2015**, *87*, 19−41.
(12) Wei, X.; Tian, T.; Jia, S.; Zhu, Z.; Ma, Y.; Sun, J.; Lin, Z.; Yang, C. J. *Anal. Chem.* **2016**, *88*, 2345−2352.
(13) Niedl, R. R.; Beta, C. *Lab Chip* **2015**, *15*, 2452−2459.
(14) Zhu, C.; Lu, Y.; Peng, J.; Chen, J.; Yu, S. *Adv. Funct. Mater.* **2012**, *22*, 4017−4022.
(15) Jadhav, A. D.; Yan, B.; Luo, R. C.; Wei, L.; Zhen, X.; Chen, C. H.; Shi, P. *Biomicrofluidics* **2015**, *9*, No. 034114.
(16) Zhu, C.; Lu, Y.; Chen, J.; Yu, S. *Small* **2014**, *10*, 2796−2800.
(17) Fu, G.; Liu, W.; Feng, S.; Yue, X. *Chem. Commun.* **2012**, *48*, 11567−11569.
(18) Mitchell, H. T.; Schultz, S. A.; Costanzo, P. J.; Martinez, A. W. *Chromatography* **2015**, *2*, 436−451.
(19) Huang, W.; Liang, Y.; Deng, Y.; Cai, Y.; He, Y. *Microchim. Acta* **2017**, *184*, 2959−2964.
(20) Liu, L.; Lin, H. *Anal. Chem.* **2014**, *86*, 8829−8834.
(21) Wang, F.; Wu, Y.; Zhan, S.; He, L.; Zhi, W.; Zhou, X.; Zhou, P. *Aust. J. Chem.* **2013**, *66*, 113−118.
(22) Purcell, T. W.; Peters, J. J. *Environ. Toxicol. Chem.* **1999**, *18*, 3−8.
(23) Zhou, D.; Zeng, K.; Yang, M. *Microchim. Acta* **2019**, *186*, 121.
(24) Ma, X.; Chen, Z.; Kannan, P.; Lin, Z.; Qiu, B.; Guo, L. *Anal. Chem.* **2016**, *88*, 3227−3234.
(25) Bi, N.; Hu, M.; Xu, J.; Jia, L. *Microchim. Acta* **2017**, *184*, 3961−3967.
(26) Farka, Z.; Cunderlova, V.; Horackova, V.; Pastucha, M.; Mikusova, Z.; Hlavacek, A.; Skladal, P. *Anal. Chem.* **2018**, *90*, 2348−2354.
(27) Dai, H.; Li, Y.; Zhang, Q.; Fu, Y.; Li, Y. *RSC Adv.* **2018**, *8*, 33960−33967.
(28) Alkilany, A. M.; Thompson, L. B.; Boulos, S. P.; Sisco, P. N.; Murphy, C. J. *Adv. Drug Delivery Rev.* **2012**, *64*, 190−199.

DOI: 10.1021/acs.analchem.9b04059
Anal. Chem. 2019, 91, 13290−13296